Oil-water displacements in rough microchannels

Bera, B.; Hauner, I.; Qazi, M.; Bonn, D.; Shahidzadeh, N.

DOI
10.1063/1.5053625
Publication date
2018
Document Version
Final published version
Published in
Physics of Fluids

Oil-water displacements in rough microchannels

Bijoyendra Bera,[a] Ines Hauner, Mohsin Qazi, Daniel Bonn, and Noushine Shahidzadeh
Soft Matter Group, Institute of Physics, Science Park 904, 1098 XH Amsterdam, The Netherlands

(Received 24 August 2018; accepted 14 October 2018; published online 1 November 2018)

We investigate the effect of wall roughness upon the entrapment of oil (alkanes) by water flooding in a microchannel. We use fluorescence microscopy to track the *in situ* oil displacement process in these channels of controlled wall roughness. We find that the viscosity contrast between water and oil determines whether the alkane phase is partially retained in the microchannel. Oil recovery rates are found to be controlled by the wall roughness and the flow rate in the experiment. We also perform the displacement experiments in novel microfluidic 2D porous networks and show that a small variation in the pore-size distribution is also a representation of the solid medium's roughness. We observe that the trapped oil in the porous network follows the same trend as in the rough microchannels, i.e., viscosity contrast, flow speed, and roughness govern the quantity of the trapped oil. We propose a scaling law to quantify the trapped fluid volume based on our experimental observations, which accounts for both the flow rate and the characteristic roughness of the system. https://doi.org/10.1063/1.5053625

INTRODUCTION

Microfluidics allows us to study fluid displacement scenarios in two phase flow/entrapment problems of many practical applications. The effect of pore-geometry and wettability on displacement of fluids is a central theme in porous media research.[1,2] This pore geometry and wettability approach encompass a number of length scales starting from nanoscale wetting at the molecular level, capillarity effects, and local contact-angle distributions at the mesoscale to macroscopic fluid flows at larger scales. A classic three-phase wetting scenario of course automatically entails the displacement of a viscous fluid by another in a porous medium. The structure of the porous material, i.e., the geometry of the intertwined pathways, and how they are connected through throat-like constrictions are known to be very important parameters. However, the surface topology, e.g., the surface roughness of the porous media, is usually not taken into account in such approaches and is ill-understood.

For example, enhanced oil recovery (EOR)[3] has received tremendous attention in the past half a century. The pore-scale wettability approach[4,5] is usually followed in such studies, but so far the effects of wall roughness have been either completely ignored or only introduced in a classic Wenzel or Cassie-Baxter argument.[6–8] The entrapped oil droplets can then be ideally recovered if the droplet on a solid phase undergoes Cassie-Baxter to Wenzel transition. This approach, however, only holds for a hydrophobic material while, in reality, many of these solid phases, especially rock surfaces in oil reservoirs, are more hydrophilic. Gravity-assisted drainage experiments in hydrophilic porous networks have been reported,[9] where wettability seems to have a large effect on the dynamics of the oil displacement process. However, roughness has not been implemented in such a study. Recently, Bertin *et al.*[10,11] have demonstrated in core-scale studies that the recovery rates of the same oil can be very different in rocks that are chemically identical but have different surface topologies, i.e., a single pore size distribution ("unimodal" core) or a double-peaked pore size distribution ("bimodal" core). In these studies, the extra oil entrapment/release in the bimodal rock core was tentatively attributed to the roughness of the rock; however, due to the nature of their experiments, this could not be verified experimentally and remains to be understood. The experimental difficulty lies in the fact that core-scale studies do not permit looking into individual pores to investigate what causes the observed effects. In micro-scale experiments, often a microchannel with regular bends[12] has been used to investigate turbulence or throttling effects, but not rough channels. Sometimes, the stability between a liquid and a gas (bubble bifurcation) is studied in a microchannel[13] or the response of particles in a shear flow.[14] However, to the best of our knowledge, there is no study in the literature attempting to quantify this roughness effect in a pore-scale experiment as well as analyze the effect in an existing theoretical framework.

In this work, we investigate the roughness effect on the displacement of oil (alkanes) by water both at the micro-scale and at the pore-scale. Studies of fluid flow in microscale roughness have thus far been limited to gas-flow experiments[15] or fluid flow simulations[16–19] mostly in hydrophobic channels.[20] We report the first evidence of roughness-dependent oil entrapment/release in both rough microchannels and porous networks. We furthermore mimic the core-scale cases of the unimodal and bimodal rocks from the work of Bertin *et al.*[10,11] in our porous networks. Subsequently, we also analyze the data to present a scaling law involving capillary effects as well as the roughness of the system.

[a]Electronic mail: b.bera@uva.nl

MATERIALS AND METHODS

Rough microchannels

Various glass microchannels representing different characteristic roughnesses are used in the experiments. Channels having a "microroughness" are prepared by powderblasting glass substrates (length 40 mm, cross section 20 μm × 50 μm), resulting in a root mean square (RMS) roughness between 1 and 3 μm, based on the hill to valley distances. Larger roughness features are realized by dry-etching repetitive "zigzag" structures on the side-walls of the glass microchannels (40 mm long, cross section 60 μm × 20 μm). As illustrated in Fig. 1, all microfluidic channels have very similar dimensions but possess roughness features of different sizes. The "zigzag" channels contain well-defined cavities of 10 and 20 μm on their respective side walls.

Porous media

Porous media can be viewed as having channels with a roughness on the order of the pore size. In order to visualize water flooding in a porous medium, two-dimensional (2D) porous networks are prepared. Glass beads (soda lime, 210-250 μm diameter, melting point 710 °C) are introduced into a micro-capillary (CM Scientific, length 50 mm, cross section 3 mm × 300 μm) sealed on one side. After filling with glass beads completely, the capillary is sealed on the other side as well and placed in a centrifuge at 3000 g for 25 min to compact the beads. Subsequently, the capillaries are placed in a programmable oven with a specific heating and cooling protocol to sinter the beads together and to the wall (see the supplementary material). In order to ensure that the beads stick to the capillary wall, the capillaries were kept under a load while sintering in the oven.

Fluids flowing through such a porous network experience channels which are wide (pores) as well as narrow (throats) on the length scale of the beads. This can be considered and viewed as a roughness and compared to the rough microchannels. Porosimetry studies show that the characteristic pore size in a porous medium is one-third of the grain size and further assume that the characteristic roughness of the medium is the same as its characteristic pore size. Since the beads are ~240 μm in diameter, the average pore size and therefore the characteristic length scale of the roughness is empirically given by one-third of this diameter, i.e., ~80 μm. If the 2D porous medium is homogenously filled, all pore sizes are roughly equal and we call these channels "unimodal" porous networks.[10,11] We fill the microchannel with water completely and measure the mass of this water to calculate the porosity of the channel. For the unimodal porous network, the porosity is found to be 30% ± 2%.

In order to mimic the heterogeneity in pore sizes present in real reservoir rocks, a second type of porous medium with two characteristic pore (roughness) sizes is prepared which we will refer to as the "bimodal" porous networks. The preparation method is similar to that for the unimodal ones, except that the microcapillaries are filled with a mixture of glass beads and NaCl salt crystals of similar size as the glass beads. The porous medium is prepared in the oven; the NaCl crystals have a melting temperature of 801 °C, which is much higher than that of glass, and thus, simply, the crystals remain in place. The capillary is subsequently immersed in warm water (~80 °C) for a period of 6 h in order to dissolve the salt crystals. The porous medium is subsequently carefully rinsed several times to remove all traces of salt and put to dry in the oven at 80 °C. Figure 2 shows the bright-field image of such a bimodal porous network with the bigger and smaller pores highlighted.

Because of its inherent heterogeneity, assessing the characteristic length scale of the roughness of the bimodal porous network is not straightforward. However, the sizes of the bigger pores are similar to each other, and we fit circles in these big pores to determine their sizes from microscopy images such as in Fig. 2. Once we have a distribution of the number and sizes of the large pores, we simply calculate the arithmetic weighted mean of all the pore sizes (one of these sizes being

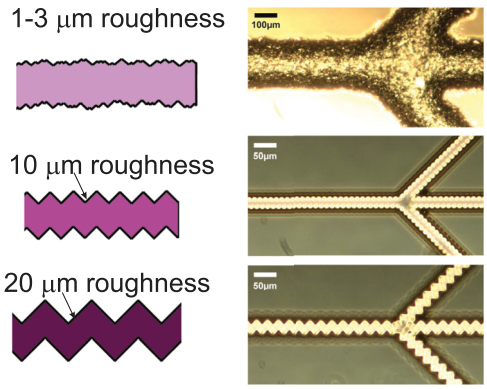

FIG. 1. **Microchannels of increasing roughness.** Left*:* Schematic top view. Right*:* Bright-field microscopy top view.

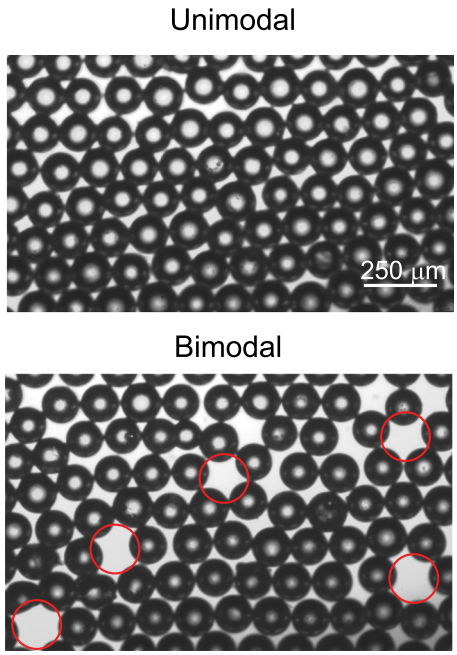

FIG. 2. **Porous media with different characteristic roughnesses.** (a) Unimodal system, with a characteristic roughness equal to the pore size which is 80 μm. (b) Bimodal system, where the bigger pores are highlighted with circles. In this case, the characteristic roughness is about 140 μm.

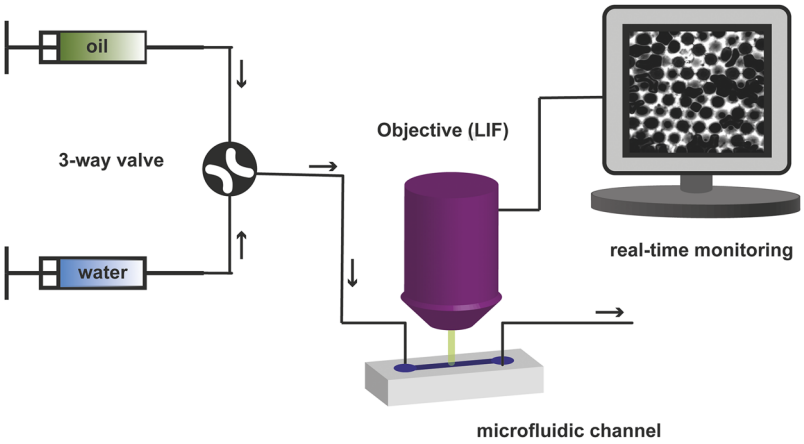

FIG. 3. **Microfluidic setup.** The displacement of one fluid (oil) in a microfluidic device by flooding with a second fluid (water) is realized using two syringe pumps connected to a 3-way valve system that allows switching between the oil and a water syringe. Laser-induced confocal fluorescent microscopy (LIF) is used for real-time monitoring of the flooding and displacement processes in the microfluidic channel.

80 μm to represent the pore size of normally packed beads) to obtain the average pore size of the bimodal porous network. This value is found to be approximately 140 μm. The porosity of the bimodal porous network, determined in the same manner as for the unimodal network, is found to be 44% ± 2%. Various details and steps of porous media fabrication have been provided in the supplementary material. Furthermore, some of us have previously published[21] the practical aspects of fabrication of the porous media shown in Fig. 2 where porosity distribution, wettability, etc., are discussed in detail.

Water flooding experiments

All water flooding experiments are performed using the microfluidic setup depicted in Fig. 3. The microchannel is connected with the water and oil reservoirs (microsyringes of volume 250 μl, Hamilton) through a 3-way valve (Stopcock 4, Cole-Parmer, USA). Initially, the microchannel/porous medium is filled with the oil phase labelled with a fluorescent dye (~1 μm perylene bisimide, Sigma-Aldrich). Subsequently, the valve is switched in order to inject the wetting fluid water in the microchannel/porous medium. The oil-displacement process is followed by a laser confocal fluorescence microscope (Zeiss LSM 5 Pascal), allowing us to obtain a complete 3D image of the oil distribution within the channels. The relative volumes of oil and water in the microchannels are calculated by image analysis of the fluorescent images. During image analysis, the x-y pixels belonging to each phase are counted (by image thresholding the two phases present) and, subsequently, the volume is calculated. The fact that the oil is trapped uniformly along the height of the channel is qualitatively confirmed using the z-scan information from the microscope.

RESULTS AND DISCUSSION

Effects of roughness and viscosity on oil recovery

First, the effect of rock roughness on oil recovery is investigated through the "water flooding" experiments in the "rough" microchannels. In these experiments, alkanes are displaced by water. We used different alkanes as the oil phase and discuss here the typical results obtained with a light alkane (decane) and a heavy one (hexadecane). The main difference between them is that the latter is more viscous than water, while the former is less viscous than water (Table I). Decane is found to be easily displaced by water in most of the microchannels. In a straight microchannel (i.e., zero roughness) and in microchannels with a characteristic roughness of 1-3 μm, 10 μm, and 20 μm, decane is completely displaced by water during the water flooding process (Fig. 4, middle). For hexadecane, however, we observe a significantly different displacement pattern. In a zero-roughness channel and in the microroughness channels (with a characteristic roughness of 1-3 μm), hexadecane is completely displaced by water (Fig. 4, top right). However, as the characteristic roughness in the channel increases (first 10 μm and then 20 μm), the amount of hexadecane trapped in the channel increases (Fig. 4, right) and the amount of recovered oil hence decreases. The size of trapped oil drops depends on the roughness as well as the volume flow rate of the displacing phase water. This is shown in Fig. 5 for a 20-μm zigzag roughness channel after the water flooding process has been completed. As the flow rate q (and hence, the capillary number Ca, given by $Ca = \eta \cdot u/\gamma$, where η is the dynamic viscosity of the displacing fluid, u is its average velocity, and γ is the interfacial tension between the two liquid phases) increases, the size of the trapped drop also increases. In Figs. 4 and 5, all the subfigures (other than the schematics in Fig. 4, left) are experimental images which show the oil water distribution after the completion of the displacement and hence represent the steady state in our system. We conclude from these experiments that if the displaced oil phase has a higher viscosity, the displacement is less efficient and some oil is left behind. This is reminiscent of the classical Saffman-Taylor instability: when a high viscosity fluid (such as oil) is displaced by a low-viscosity fluid (such as water), the interface is unstable and the "fingers" of the displacing fluid propagate, leaving some of the displaced fluid behind.[22–24] This is shown schematically in Fig. 6(a). Following the perturbation analysis presented by Saffman and Taylor,[22,25] the critical wavelength

TABLE I. Properties of the fluids (at 20 °C) used in this study.

Property	Water	Decane	Hexadecane
Density (ρ, kg/m^3)	997	730	770
Viscosity (η, Pa s)	10×10^{-4}	9.2×10^{-4}	3×10^{-3}
Inter. ten. (γ, mN/m)	...	50	46
Contact angle (θ, deg)	23	~0	~0

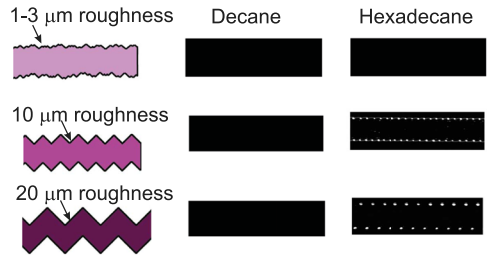

FIG. 4. **Water flooding experiments.** Fluorescence imaging reveals significant differences (flooding flowrate = 250 nl/min) between the trapping behavior of (fluorescently labelled) oils with different viscosities in microchannels with different roughness feature sizes. The inviscid decane (η = 0.92 mPa s) is not retained under any of the tested experimental conditions, whereas considerable amounts of the more viscous hexadecane (η = 3.47 mPa s) remained trapped in roughness features of at least 10 μm in size. t_{end} is typically 1 hr after the start of the experiment. The entire range of droplet diameters in a representative experiment has been presented in the supplementary material along with their distribution.

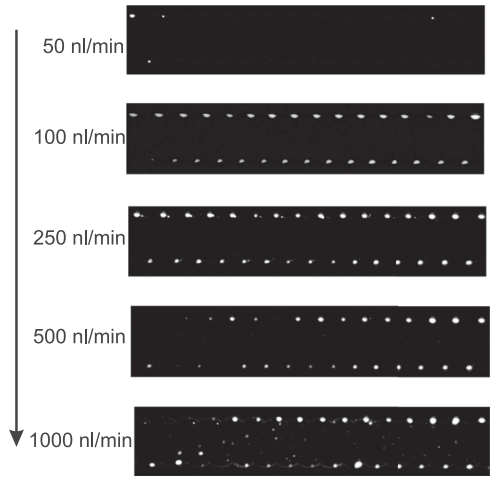

FIG. 5. **Flowrate dependence of oil trapping.** Fluorescence images of hexadecane oil droplets trapped in a rough microchannel of the "zigzag 20" type, which has a 20 μm characteristic roughness, as a function of the water flooding floodrate. The average size of the trapped oil droplets is seen to increase when the flowrate is increased from 50 to 1000 nl/min.

of this viscous finger (λ_c) is given by $\lambda_c = \pi b\sqrt{\frac{\gamma}{\Delta\eta U}}$, where b is the width of the channel, γ is the interfacial tension between the two fluids, $\Delta\eta$ is the difference in fluid viscosities, and U is the flow velocity. We note here that a smaller λ_c implies a more unstable finger and eventual pinch-off and formation of the trapped droplet of the phase with higher viscosity. It follows immediately that an increase in the viscosity difference $\Delta\eta$ will lead to a smaller λ_c and hence larger trapped oil droplets as observed in Fig. 4 between decane and hexadecane. Decane actually has a lower viscosity than water, and an unstable viscous finger does not form at all in the case of decane. Similarly, increasing the flow velocity U results in a smaller λ_c and bigger trapped droplets, as shown in Fig. 5. Finally, the roughness effect can also be explained from this relation. By introducing the zigzag roughness in the microchannel, we reduce the effective width b of the microchannel, which, in turn, reduces λ_c. Hence, increasing the length of the zigzag part directly helps in the formation of larger trapped droplets which is exactly what we observe here for the hexadecane case in the channel.

Porous networks

In order to generalize the effect of roughness on oil displacement in a porous medium, we now investigate the 2D porous networks. As in the case of the microchannel experiments, the viscosity is found to play an important role: in a unimodal porous network with a characteristic pore-size of ~80 μm, more hexadecane [Fig. 7(a)] remains trapped than decane (shown in the supplementary material) after water flooding. The same trend of oil displacement/entrapment is found for the bimodal porous networks: more decane is trapped in the bimodal porous network compared to the unimodal porous network. For hexadecane, the relative amount of trapped oil in the bimodal porous network is the largest among all our experiments. Figures 7(b) and 7(c) show the decane and hexadecane displacements, respectively, in bimodal porous networks. Decane is displaced in a more uniform manner from the entire length of the channel, while hexadecane seems to remain trapped in various small or large pores. The heterogeneity of the porous network also influences the oil displacement. It is clear from Figs. 7(b) and 7(c) that the majority of oil is displaced from the big pores in the bimodal porous network even though the total amount of oil recovery is less in the case of the bimodal network compared to other microchannels. This implies that for a bimodal network, most of the oil trapped in between the glass beads is not recoverable.

Capillary scaling

As a measure of the oil entrapment after water flooding in both the microchannels and the porous networks,

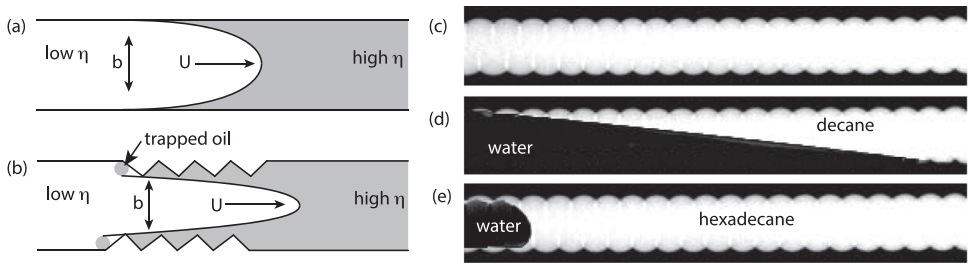

FIG. 6. **Saffman-Taylor instability.** (a) A schematic of a viscous finger formation when a fluid of lower viscosity displaces a fluid with higher viscosity. (b) Increasing the roughness of the wall helps reduce the critical wavelength λ_c of the viscous finger, facilitating the formation of trapped droplets. (c) Zigzag microchannels filled with fluorescent oil before water flooding. (d) When decane is displaced with water, there is no viscous finger formed, while (e) hexadecane displacement by water leads to a viscous finger.

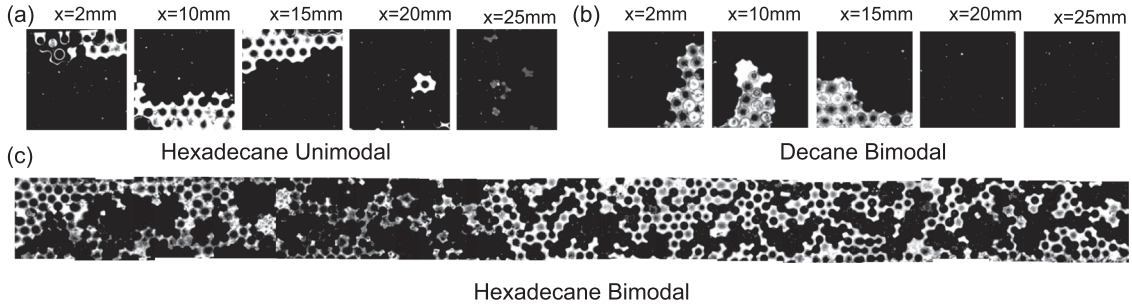

FIG. 7. **Dynamics of displacement.** Fluorescent images after water flooding of porous networks originally filled with either hexadecane or decane. Similar to the case of the rough microchannels, the images are taken hours after the conclusion of the displacement process, i.e., after the oil water phases in the microchannel are in an equilibrium state. The images are taken at various locations of the porous network where x denotes the distance from the inlet. (a) Hexadecane flooding from a unimodal channel; (b) decane flooding from a bimodal channel; (c) hexadecane flooding from a bimodal channel; individual images are combined to present an overview of the entire channel. The total length of the channel is 2 cm.

we determine the diameter of the trapped oil droplet d_{oil} (in the case of the microchannels, where the remaining oil is in the form of drops of a regular geometric shape) or the area of the trapped oil A_{oil} (in the case of the porous networks, where the oil is in the form of random blobs) by analyzing the fluorescent images. We observe that the drop diameter d_{oil} or the square root of A_{oil} for trapped hexadecane vs the volume flow rate q follows a power law $d_{oil} \sim q^n$ with $n = 1/3$. The insets of Fig. 8 show the $q^{1/3}$ fitting for trapped hexadecane in 10-μm and 20-μm zigzag microchannels. This power law is reminiscent of the classic Bretherton's problem of a droplet trapped in a circular capillary or a Hele-Shaw cell,[26] where pressure-driven flow results in the exact same power law for the thickness of the film left behind on the wall.[27,28] In order to include the roughness of the microchannel in the scaling law, we introduce the parameter d_{oil}/r (or $\sqrt{A_{oil}}/r$), where r is the characteristic roughness of the microchannel (Fig. 8). The resulting trend still follows the same power law of $\frac{1}{3}$. Moreover, the roughness-normalized data for the zigzag channels and for the two types of porous networks collapse onto a single curve within the range of experimental error. This indicates that we

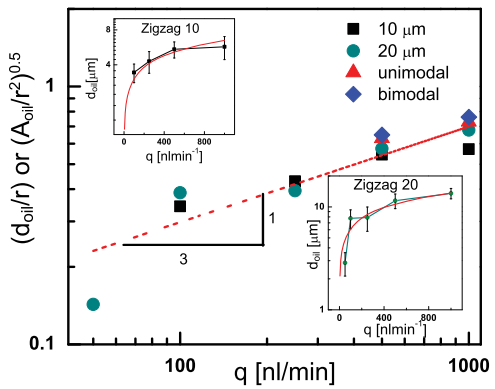

FIG. 8. **Size of the trapped oil droplets.** Insets: The average diameter d_{oil} of the trapped hexadecane oil droplets increases with increasing water flooding flowrate q in both the 10-μm (black squares connected by black lines) and 20-μm (green circles connected by green lines) zigzag channels. The red solid lines are fits to a $q^{1/3}$ dependency. Main graph: Trapped oil droplet diameter (or square root of the oil area A_{oil} in porous networks as determined from fluorescence images) normalized to the channel roughness r. The data collapse onto a single dependency. As indicated by the slope of the dotted red line, the normalized parameter also scales with $q^{1/3}$.

can gain insight regarding the physical principle of oil recovery from porous media using model microfluidic experiments on rough channels. This is the main result of our study and is to the best of our knowledge the first time it has been reported. It is important to note that our results are very specific to the wetting properties of the liquids used in these experiments. It has been shown previously that the wetting properties of the fluids can lead to a modification of this scaling law even for a Hele-Shaw cell.[29] Hence, without any doubt, the wetting of a more complex flow cell such as our microchannels or the porous networks will also have a strong influence on the overall oil entrapment and its scaling analysis. This is especially the case in the porous network, where the difference between an imbibition or a drainage experiment leads to the so-called *ink-bottle effect*.[30] It is a well-established fact that the imbibition process is governed by the radius of the large pores while the drainage process is led by the throats, i.e., the constrictions connecting these bigger pores leading to a capillary hysteresis.

Our results imply that the characteristic roughness of a microchannel can be incorporated in a scaling relation for the trapped oil drop diameter with the capillary number Ca that compares the flow velocity to the capillary velocity γ/η with γ being the surface tension and η being the viscosity. However, since the data collapse as a function of the flow rate and the capillary velocities of the hexadecane and decane are different, the data will not collapse when plotted against the capillary number. This is most probably due to the fact that the capillary number uses the absolute viscosity η of the fluid, while the roughness effect follows from the Saffman-Taylor instability analysis, where the relevant parameter is the viscosity difference $\Delta\eta$. In other words, if we displace water with a fluid of viscosity approximately 3 times smaller than water, then the trapped water drop diameters will still be the same as observed in our experiments for trapped oil, but the combined capillary/roughness fitting will no longer satisfy a classic power law, since the absolute value of the viscosity (of the displacing liquid) is almost an order of degree different than hexadecane. Hence we can conclude that the scaling law presented in this work is quite unique for the particular fluids as well as the channel- and roughness-dimensions used in our experiments. In addition, capillary effects are dominated by interfacial tension as seen clearly from the expression of Saffman Taylor

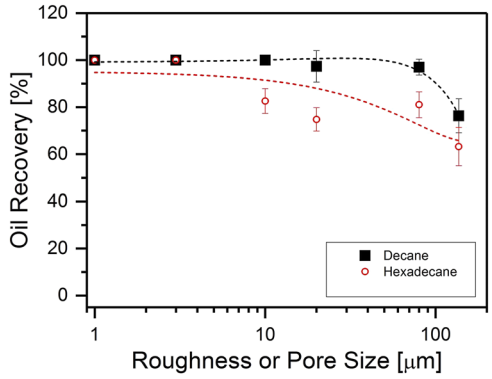

FIG. 9. **Oil recovery efficiency vs characteristic roughness.** Fraction of oil recovered from the rough microroughness channels, zigzag channels, and porous networks, calculated from analyzing fluorescence images, as a function of the characteristic roughness for two types of oils. The error bars signify the standard deviation of calculated oil recovery based on five independent experiments. In order to allow for a comparison between the microchannels and the 2D porous networks, the oil recovery for the microroughness and zigzag systems is calculated based on the volume where the oil is trapped, i.e., the zigzag part only. The volume of the straight part (in the center) of the microchannel, where no oil is trapped, is subtracted from the total microchannel volume. The dotted lines are guides to the eye. The flow rate is $q = 500$ nl/min.

instability. The alkanes used in our experiments have comparable surface tension, and hence, its effect is negligible. By changing the surface tension of the fluids used, one could probe deeper into the capillary effects in oil displacement. However, this is beyond the scope of the current paper, since here we focus on the viscosity contrast.

Finally, in Fig. 9, we summarize our results in terms of the overall oil recovery efficiency as a function of characteristic roughness (i.e., roughness of the channels or average pore size of the porous systems) for decane and hexadecane. The fraction of recovered oil is dependent on the size of the roughness features and the viscosity of the displaced oil. Decane has a lower viscosity than water (Table I) and is easily driven out of the system under our experimental conditions. Hexadecane has a roughly four times higher viscosity and significant amounts remain trapped in the rough channels with increasing size of the roughness features. The data shown in Fig. 9 are all at a flow rate of $q = 500$ nl/min. These values will be different at a different flow rate since we have shown in the section titled Results that the amount of oil recovery depends on the water flooding flowrate. Here, it is important to note that the flow rates used in our experiments are higher than the typical water flooding rates used in petroleum industry (usually 1 ft/day). Our experimental system is inspired by many different practical applications and is designed to investigate the generic nature of light oil displacement by water. Hence, a specific focus on the oil recovery application will require further studies with lower water flooding rates which is beyond the scope of the current work.

CONCLUSIONS

We have investigated the influence of roughness on oil displacement by water in microchannels. This study encompasses a range of roughnesses, starting from small-scale roughness (1-3 μm) in a simple microchannel to a complex porous network where we control the average pore diameter (80-140 μm) of the network, which is representative of the characteristic roughness of the medium. The displacement of oil by water is found to depend on the viscosity of the oil as expected, but more importantly, on the characteristic roughness of the channel. Oil entrapment increases with an increasing roughness. We find that the trapped oil droplet diameter (or the square root of the trapped oil area) normalized by the characteristic roughness scales with the cube root of the water flooding floodrate. Usually, the fluid entrapment or fingering effects in a microchannel are attributed to the capillary effects. Our study shows, for the first time, that roughness has an equally big impact on the fluid flow properties in a microchannel. We have also incorporated the roughness in a generic scaling argument involving surface tension and viscosity. In considering the dynamics of displacement processes in a porous or a disordered medium, roughness should therefore be considered as well.

SUPPLEMENTARY MATERIAL

See supplementary material for the following points: (1) Fabrication of porous network, (2) characterization of the porous network, (3) methods of image analysis, (4) size distribution of trapped oil droplets in microchannels, and (5) decane displacement by water from a unimodal porous network.

[1]M. J. Blunt, "Flow in porous media pore-network models and multiphase flow," Curr. Opin. Colloid Interface Sci. **6**, 197–207 (2001).
[2]M. J. Blunt and H. Scher, "Pore-level modeling of wetting," Phys. Rev. E **52**, 6387–6403 (1995).
[3]D. W. Green and G. P. Willhite, *Enhanced Oil Recovery*, SPE Textbook Series (Henry L. Doherty Memorial Fund of AIME, Society of Petroleum Engineers, 1998).
[4]N. Gunda, B. Bera, N. K. Karadimitriou, S. K. Mitra, and S. M. Hassanizadeh, "Reservoir-on-a-chip (roc): A new paradigm in reservoir engineering," Lab Chip **11**, 3785–3792 (2011).
[5]N. Sefrioui, A. Ahmadi, A. Omari, and H. Bertin, "Numerical simulation of retention and release of colloids in porous media at the pore scale," Colloids Surf., A **427**, 33–40 (2013).
[6]D. Bonn, J. Eggers, J. Indekeu, J. Meunier, and E. Rolley, "Wetting and spreading," Rev. Mod. Phys. **81**, 739–805 (2009).
[7]D. Bonn and D. Ross, "Wetting transitions," Rep. Prog. Phys. **64**, 1085 (2001).
[8]P. G. de Gennes, F. Brochard-Wyart, and D. Quere, *Capillarity and Wetting Phenomena: Drops, Bubbles, Pearls, Waves* (Springer, New York, 2003).
[9]N. Shahidzadeh-Bonn, A. Tourni, S. Bichon, P. Vi, S. Rodts, P. Faure, F. Bertrand, and A. Azouni, "Effect of wetting on the dynamics of drainage in porous media," Transp. Porous Media **56**, 209–224 (2004).
[10]F. Nono, H. Bertin, and G. Hamon, "An experimental investigation of the oil recovery in the transition zone of carbonate reservoirs taking into account wettability change," in Proceedings of International Petroleum Technology Conference, Doha, Qatar, 20–22 January 2014.
[11]F. Nono, H. Bertin, and G. Hamon, "Oil recovery in the transition zone of carbonate reservoirs with wettability change: Hysteresis effects of relative permeability versus experimental data," in Proceedings of International Symposium of the Society of Core Analysts, Avignon, France, 8–11 September 2014.
[12]W. Liu, G. Tang, W. Su, L. Wu, and Y. Zhang, "Rarefaction throttling effect: Influence of the bend in micro-channel gaseous flow," Phys. Fluids **30**, 082002 (2018).
[13]Y. Shen, L. Hu, W. Chen, and X. Fu, "Periodic and aperiodic bubbling in submerged gas-liquid jets through a micro-channel," Phys. Fluids **29**, 047104 (2017).

[14]J. Fries, M. V. Kumar, B. M. Mihiretie, D. Hanstorp, and B. Mehlig, "Spinning and tumbling of micron-sized triangles in a micro-channel shear flow," Phys. Fluids **30**, 033304 (2018).
[15]Z. Deng, Y. Chen, and C. Shao, "Gas flow through rough microchannels in the transition flow regime," Phys. Rev. E **93**, 013128 (2016).
[16]B.-Y. Cao, M. Chen, and Z.-Y. Guo, "Rarefied gas flow in rough microchannels by molecular dynamics simulation," Chin. Phys. Lett. **21**, 1777 (2004).
[17]O. I. Rovenskaya and G. Croce, "Numerical simulation of gas flow in rough microchannels: Hybrid kinetic continuum approach versus Navier Stokes," Microfluid. Nanofluid. **20**, 81 (2016).
[18]S. Shen, J. L. Xu, J. J. Zhou, and Y. Chen, "Flow and heat transfer in microchannels with rough wall surface," Energy Convers. Manage. **47**, 1311–1325 (2006).
[19]D. Y. Yang, "Numerical analysis of micro-mixing in rough microchannels," in *Manufacturing Process Technology*, Advanced Materials Research, Vol. 189 (Trans Tech Publications, 2011), pp. 1452–1455.
[20]C. Kunert and J. Harting, "Simulation of fluid flow in hydrophobic rough microchannels," Int. J. Comput. Fluid Dyn. **22**, 475–480 (2008).
[21]R. W. Liefferink, A. Naillon, D. Bonn, M. Prat, and N. Shahidzadeh, "Single layer porous media with entrapped minerals for microscale studies of multiphase flow," Lab Chip **18**, 1094–1104 (2018).
[22]P. Saffman and G. Taylor, "The penetration of a fluid into a porous medium or hele-shaw cell containing a more viscous liquid," Proc. R. Soc. London, Ser. A **245**, 312–329 (1958).
[23]R. M. Oliveira and E. Meiburg, "Saffman-Taylor instability and the inner splitting mechanism," Phys. Rev. Lett. **118**, 124502 (2017).
[24]D. Bonn and J. Meunier, "Viscoelastic free-boundary problems: Non-Newtonian viscosity vs normal stress effects," Phys. Rev. Lett. **79**, 2662–2665 (1997).
[25]Y. Couder, "Viscous fingering as an archetype for growth patterns," in *Perspectives in Fluid Dynamics: A Collective Introduction to Current Research*, edited by G. Batchelor, H. Moffatt, and M. Worster (Cambridge University Press, 2002), pp. 53–104.
[26]C.-W. Park and G. M. Homsy, "Two-phase displacement in hele shaw cells: Theory," J. Fluid Mech. **139**, 291–308 (1984).
[27]A. Huerre, O. Theodoly, A. M. Leshansky, M.-P. Valignat, I. Cantat, and M.-C. Jullien, "Droplets in microchannels: Dynamical properties of the lubrication film," Phys. Rev. Lett. **115**, 064501 (2015).
[28]J. Seiwert, C. Clanet, and D. Quéré, "Coating of a textured solid," J. Fluid Mech. **669**, 55–63 (2011).
[29]E. Álvarez-Lacalle, J. Ortín, and J. Casademunt, "Relevance of dynamic wetting in viscous fingering patterns," Phys. Rev. E **74**, 025302 (2006).
[30]O. Coussy, *Mechanics and Physics of Porous Solids* (Wiley, 2011).